Dzyaloshinskii-Moriya interaction transistor with magnetization manipulated by electric field

Cheng Ma,[1,2] Kui-Juan Jin,[1,2,*] Er-Jia Guo,[1,2] Chen Ge,[1,2] Can Wang,[1,2] and Xiu-Lai Xu[1,3]
[1] *Institute of Physics, Chinese Academy of Sciences, Beijing 100190, China*
[2] *University of Chinese Academy of Sciences, Beijing 100049, China*
[3] *State Key Laboratory for Mesoscopic Physics and Frontiers Science Center for Nano-optoelectronics, School of Physics, Peking University, Beijing 100871, China*

(Received 31 May 2024; accepted 23 August 2024; published 11 September 2024)

Electric-field control of magnetization is crucial for next-generation spintronic devices with reduced energy consumption and increased integration density. Based on magnetoelectric multiferroics whose Dzyaloshinskii-Moriya interaction (DMI) vectors are coupled to their polarization, we propose the architecture of a DMI transistor which utilizes voltage-controlled DMI torque to reverse the magnetization orientation, enabling current-free magnetization reversal. By leveraging the properties of a CrN monolayer, we demonstrate the feasibility of the DMI transistor through first-principles calculations, micromagnetic simulations, and analytical calculations. We find that the switching time of the DMI transistor (in subnanoseconds) increases with the exchange interaction and decreases with the DMI. We also show how the size of the DMI transistor (in nanometers) depends on the exchange interaction and the DMI and how it can be further tuned by the magnetic anisotropy. In this paper, we pave the way toward highly desired electric-field control and current-free ultrafast spintronic devices, with the potential toward logic-in-memory architecture overcoming the von Neumann bottleneck.

DOI: 10.1103/PhysRevB.110.094418

I. INTRODUCTION

To meet the ever-increasing demand for information storage and processing, next-generation microelectronic devices with reduced energy consumption, increased operational speed, and higher integration density are imperative to be developed [1,2]. Utilizing the spin degree of freedom of electrons, spintronic devices are expected to be promising candidates due to their advantages in terms of modulation and detection [3,4]. In spintronic devices, a bit of data is encoded in the magnetization orientation of a ferromagnetic (FM) layer (free layer) and decoded with a reference FM layer by means of giant or tunneling magnetoresistance effect, where the resistance varies dramatically while reversing the magnetization orientation of free layer [5,6]. In the current context, magnetic random-access memory based on spin-transfer torque and spin-orbital torque has achieved commercial success [7]. However, these devices rely on the charge current to flip the magnetization, inevitably resulting in Joule heating. Therefore, to further reduce the energy consumption, writing magnetic information by means of charge-current-free ways, such as by electric fields, has become a hot topic in modern physics.

Electric-field control of magnetization can be achieved through strategies such as magnetic anisotropy modification by means of strain engineering in heterostructures composed of FM and piezoelectric layers [8–11]. Moreover, taking advantage of magnetoelectric (ME) multiferroics, the interfacial magnetic exchange bias in FM/ME heterostructures can be reversely tuned by applying electric fields on the ME layer, leading to the magnetization reversal of the FM layer [12–16]. Recently, the Dzyaloshinskii-Moriya interaction (DMI) has started to show its potential to reduce the device size and increase the switching speed with strain pulse [17], magnetic field, or charge current [18]. Building on the progress of ME multiferroics or heterostructures whose DMI vectors are coupled to their polarization, it has been suggested that consequential voltage-controlled reversal of the DMI vector can lead to the transition from a skyrmion state to a quasiuniform FM state with reversed magnetization [19]. However, the reproducible switching of magnetization requires the restimulation of skyrmions by local heating [20] or spin-polarized current [21], which greatly increases the complexity and energy cost.

Inspired by the above works and other relative reports [22–27], we propose the conception of a DMI transistor which enables the reproducible voltage control of magnetization by utilizing the DMI torque to reverse the chirality of the spin spiral and the magnetization. The feasibility of this DMI transistor will be demonstrated in a specific material with a reversible DMI vector, the CrN monolayer, through a combination of first-principles calculations, micromagnetic simulations, and analytical calculations. We will show the advances of the DMI transistor in switching speed (in subnanoseconds) and in size (in nanometers), depending on the magnetic properties of the ME material.

II. RESULTS

The critical component of the DMI transistor is the spiral magnetic order in the ME material, whose chirality is determined by the DMI and exchange interaction. Therefore, we start by considering a one-dimensional (1D) magnetic chain propagating along the x axis with a lattice constant a. The

*Contact author: kjjin@iphy.ac.cn

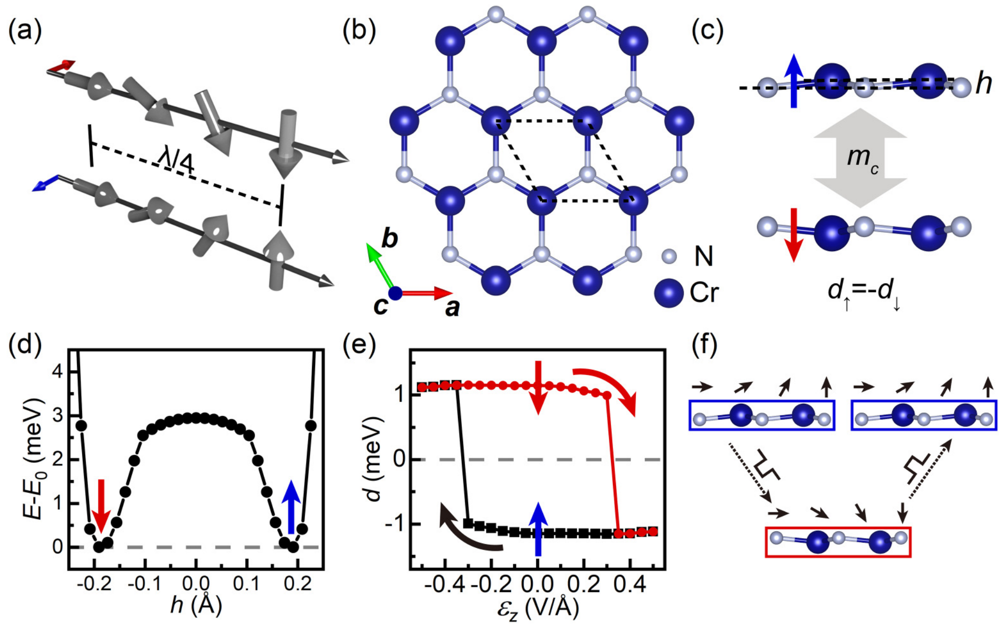

FIG. 1. (a) Diagram of spin spiral states with opposite Dzyaloshinskii-Moriya interaction (DMI) vectors, where the spins on the left side are fixed toward the x axis, and those on the right side are parallel and antiparallel to the z axis, respectively. (b) and (c) Top and side views of the CrN monolayer with two polarization states ↑ and ↓, which can be converted to each other by m_c. (d) Nudged elastic band of the CrN monolayer as a function of h, which is defined as the relative height between the Cr layer and the N layer along the c axis. (e) DMI hysteresis loop of the CrN monolayer. (f) The polarization state is switched by a pulsed electric field, and the spin on the right side also flips.

spins are assumed to lie in the xz plane, and the unit vectors can be written as $\mathbf{S}(x) = \cos\theta\mathbf{e}_z + \sin\theta\mathbf{e}_x$, where $\theta(x)$ denotes the orientation of the spin with respect to the z axis. The Hamiltonian reads as

$$H = -\sum_{\langle i,j\rangle} \mathbf{d}_{ij}\cdot(\mathbf{S}_i \times \mathbf{S}_j) - J\sum_{\langle i,j\rangle} \mathbf{S}_i\cdot\mathbf{S}_j, \qquad (1)$$

where the first term refers to the DMI characterized by the vector $\mathbf{d}_{ij}$, the second term refers to the Heisenberg exchange interaction characterized by the constant J, $\mathbf{S}_i$ and $\mathbf{S}_j$ denote the unit spin vectors on sites i and j, respectively, and $\langle i, j\rangle$ denotes the nearest-neighboring magnetic atom pairs. To be noted, since the spins are confined in the xz plane, only the y component of $\mathbf{d}_{ij}$ is relevant. Therefore, the DMI vector $\mathbf{d}$ can be written as $d\mathbf{e}_y$, with a constant d denoting the strength of DMI. This simplified atomic model allows us to gain insights into the fundamental physics of the DMI transistor. The DMI prefers right- or left-handed canted alignment of neighboring spins, while the Heisenberg exchange interaction favors parallel or antiparallel alignment. The competition between these two interactions gives rise to a homogenous spin-spiral magnetic ground state with a fixed angle $\Delta\theta$ between the neighboring spins. The energy density as a function of $\delta\theta$ is given by

$$\varepsilon(\Delta\theta) = \frac{-J\mathbf{S}^2\cos\Delta\theta - d\mathbf{S}^2\sin\Delta\theta}{a}, \quad \Delta\theta \in (-\pi, \pi]. \quad (2)$$

Therefore, $\Delta\theta$ for the magnetic ground state should meet

$$\frac{d\varepsilon}{d(\Delta\theta)} = \frac{\mathbf{S}^2}{a}(J\sin\Delta\theta - d\cos\Delta\theta) = 0, \qquad (3a)$$

$$\frac{d^2\varepsilon}{d(\Delta\theta)^2} = \frac{\mathbf{S}^2}{a}(J\cos\Delta\theta + d\sin\Delta\theta) > 0. \qquad (3b)$$

Equation (3a) gives rise to $\tan\Delta\theta = \frac{d}{J}$, which yields two solutions $\Delta\theta_{\min}$ and $\Delta\theta_{\max}$ in the given domain. Here, $\Delta\theta_{\min}$ satisfies the condition in Eq. (3b) and corresponds to the minimum value of ε, while $\Delta\theta_{\max}$ dissatisfies the condition in Eq. (3b) and corresponds to the maximum value of ε. In the case of FM coupling ($J > 0$), $\Delta\theta_{\min}$ lies in the range $(0, \pi/2)$ for $d > 0$ and $(-\pi/2, 0)$ for $d < 0$ (see the Supplemental Material [28] for the proof, see also Refs. [29–33] therein). Consequently, the magnetic ground state can be expressed as $\mathbf{S}(x) = \cos(\frac{2\pi x}{\lambda} + \theta_0)\mathbf{e}_z + \sin(\frac{2\pi x}{\lambda} + \theta_0)\mathbf{e}_x$, where the magnitude of $\lambda = \frac{2\pi a}{\Delta\theta_{\min}}$ represents the wavelength of the spin spiral with a positive value denoting clockwise rotation and vice versa, while θ_0 represents the initial phase. Particularly, when the 1D magnetic chain is with the length of $|\lambda|/4$ and the initial phase of $\theta_0 = \pi/2$, as shown in Fig. 1(a), the orientation of the spin in the right side would be parallel or antiparallel to the z axis for $d > 0$ or $d < 0$, respectively. In other words, by reversing the DMI vector, the magnetization orientation can be 180° reversed deterministically.

Since the reversal of the DMI vector controlled by an electric field has been implemented theoretically and experimentally [16,34–40], we apply the above conception in a specific material, the CrN monolayer, for demonstration. As illustrated in Fig. 1(b), the CrN monolayer, which is predicted to be a two-dimensional FM and ferroelectric (FE) multiferroics [26,31], features a hexagonal arrangement of Cr and N atoms, stacking as two atomic layers. The lattice vectors of the CrN monolayer in this paper take the form of:

$$\begin{vmatrix}\mathbf{a}\\ \mathbf{b}\\ \mathbf{c}\end{vmatrix} = \begin{vmatrix} a & 0 & 0\\ a\cos\frac{2\pi}{3} & a\sin\frac{2\pi}{3} & 0\\ 0 & 0 & c\end{vmatrix}\begin{vmatrix}\mathbf{x}\\ \mathbf{y}\\ \mathbf{z}\end{vmatrix}, \qquad (4)$$

where a and c represent the in-plane and out-of-plane lattice constants, respectively. Given that a mirror plane m_a exists in each pair of nearest-neighboring Cr atomic pairs, the DMI vector $\mathbf{d}_{ij}$ can be described as $\mathbf{d}_{ij} = d_{||}(\mathbf{e}_c \times \mathbf{e}_{ij}) + d_{\perp}\mathbf{e}_c$ according to Moriya's rules [41], where $\mathbf{e}_{ij}$ denotes the unit vectors along two magnetic atoms sited in i and j, and $\mathbf{e}_c$ denotes that along the c axis. For simplicity, we consider the in-plane component $d_{||}$ only, which gives rise to the Néel-type propagation of the spin spiral, adhering to our previous assumption for the 1D atomic model. The Cr and N atomic layers are spatially staggered, giving rise to an out-of-plane polarization. Therefore, we calculate the nudged elastic band by defining the relative height between the Cr and N layers along the c axis as h. As depicted in Figs. 1(c) and 1(d), the system exhibits two energetically degenerate ground states labeled as $\uparrow$ (up-polarized) and $\downarrow$ (down-polarized), separated by a ~ 3 meV potential barrier. The presence of the potential barrier between the states $\uparrow$ and $\downarrow$ enables the polarization to maintain or be reverse by a finite out-of-plane electric field, resulting in an electrical hysteresis loop as well as a DMI hysteresis loop, as illustrated in Fig. 1(e), where the DMI constant d is extracted by means of mapping the energies of the CrN monolayer with a real-space spin-spiral configuration in our first-principles calculations to the Hamiltonian of the DMI term [42]. Under each electric field, the lattice structure is relaxed with two initial states $\uparrow$ and $\downarrow$, and the final states with two opposite polarizations can be obtained within the range of the coercive field ~ 0.3 V/Å (like the previous work [35]). It is worth noting that the states $\uparrow$ and $\downarrow$ can be converted into each other by a mirror plane m_c, resulting in the opposite DMI vectors, i.e., $d_{\uparrow} = -d_{\downarrow}$ (see the Supplemental Material [28] for the proof). On the other hand, the Heisenberg exchange interaction, characterized by the exchange constant J, is identical for the states $\uparrow$ and $\downarrow$, i.e., $J_{\uparrow} = J_{\downarrow}$. The calculated DMI and exchange constants for the states $\uparrow$ and $\downarrow$ are $d_{\uparrow} = -d_{\downarrow} = 1.15$ meV and $J_{\uparrow} = J_{\downarrow} = 55.4$ meV, respectively, leading to a wavelength of $\lambda_{\uparrow} = -\lambda_{\downarrow} = 96$ nm.

Consequently, in a CrN nanoline with the length of $|\lambda|/4$, if the spin on the left side is pinned toward the x axis (by means of exchange bias), the spin on the right side would be out-of-plane polarized. The z component of spin S_z would be determined by the sign of d, which is governed by the polarization of CrN and controlled by the out-of-plane electric field ε_z. As illustrated in Fig. 1(f), the polarization state is switched by a pulsed electric field, and the spin on the right side also flips. To be noted, the electric field is used only to switch the polarization state, and it will be removed after the switching.

To demonstrate the basic architecture of the DMI transistor, the diagram is depicted in Fig. 2(a), where the left and right panels denote states 1 and 0 for the DMI transistor, respectively. The blue and red regions refer to the CrN monolayers with the states $\uparrow$ and $\downarrow$, respectively. On the left of the DMI transistor, a fixed layer plays the role of pinning the initial phase of the spin spiral by means of exchange bias. On the right of the DMI transistor, a free layer is FM coupled with the spin spiral serving as the source electrode (S), which consists of a magnetic tunneling junction (MTJ) combined with a space layer and a reference layer serving as the drain electrode (D). For the state $\uparrow$, the spin rotates counterclockwise, while the magnetization on the right side and that in the source electrode are parallel to the magnetization in the drain electrode, leading to a low resistance denoting 1, while for the state $\downarrow$, the reverse applies. The pulsed voltage applied on the gate electrode can switch the polarization state of the CrN monolayer, hence switching the magnetization of the source electrode and the state of the DMI transistor. Here, we define positive and negative electric-field inputs as 0 and 1, respectively. Consequently, the corresponding outputs of the DMI transistor are 1 and 0, respectively. Furthermore, by connecting the MTJs of two DMI transistors in parallel, a Not AND (NAND) logical gate can be constructed [see Fig. 2(b)]. Namely, the output of the NAND logical gate will be 0 only if the two inputs are both 1 (in state $\downarrow$ with high resistance 0). Similarly, a Not OR (NOR) logical gate can be constructed by connecting the MTJs of two DMI transistors in series [see Fig. 2(c)]. In other words, the output of the NOR logical gate will be 1 only if the two inputs are both 0 (in state $\uparrow$ with low resistance 1). Considering that the NOR and NAND gates constitute a complete set for binary operations, the DMI transistor holds the potential to serve as the basic unit of a computing system. Moreover, the nonvolatility provides the DMI transistor potential toward logic-in-memory architecture that can overcome the von Neumann bottleneck.

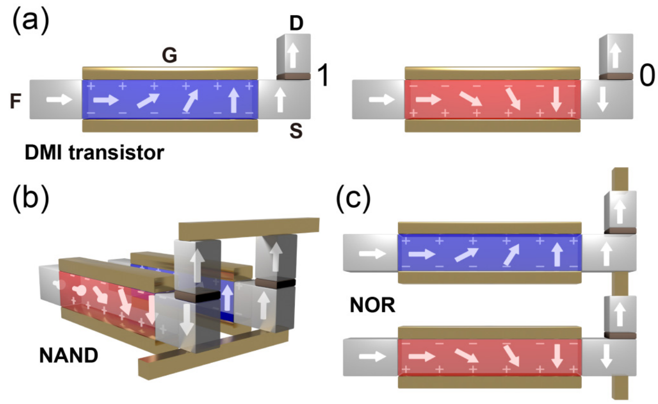

FIG. 2. (a) Diagram of the Dzyaloshinskii-Moriya interaction (DMI) transistor, where the blue and red regions refer to the CrN monolayer with the states $\uparrow$ and $\downarrow$, corresponding to low and high resistance (1 and 0), respectively. The polarization state of the CrN monolayer can be switched through the gate electrode (G). On the right of the DMI transistor, a magnetic tunneling junction (MTJ) is constructed with a reference layer and a free layer serving as the drain electrode (D) and source electrode (S). A fixed layer (F) is set on the left side. (b) and (c) NAND and NOR logical gates constructed by connecting the MTJs of two DMI transistors in parallel and in series, respectively.

Afterwards, we perform micromagnetic simulation to validate our analysis. A nanoline is set with the length of $|\lambda|/4 = 24$ nm, and the magnetization of the left side is fixed with $\theta = \pi/2$, where the DMI and Heisenberg exchange interaction are both considered. For simplicity, the long-range dipolar interaction is ignored in this size-limited 1D case. Nevertheless, the demagnetization can be approximately considered as an effective magnetic anisotropy, which considers the shape anisotropy [43]. The total-energy functional of the

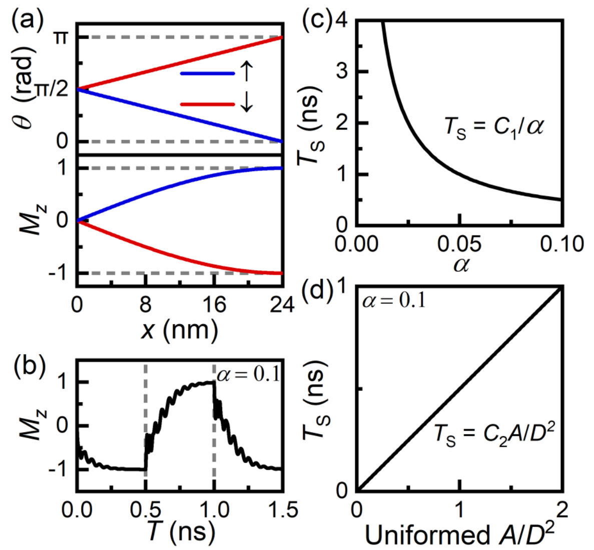

FIG. 3. Micromagnetic simulation results. (a) θ and M_z as a function of x. (b) Magnetization dynamics with $\alpha = 0.1$, where reproducible magnetization reversal can be achieved in 0.5 ns. (c) T_S as a function of α. (d) T_S as a function of A/D^2, with $\alpha = 0.1$, where the value for the CrN monolayer is uniformed as 1.

unit local magnetization $\mathbf{M}(\mathbf{r})$ reads as

$$E[\mathbf{M}(\mathbf{r})] = \int_V \{D[M_z(\nabla \cdot \mathbf{M}) - (\mathbf{M} \cdot \nabla)M_z] + A(\nabla \mathbf{M})^2\} dr^3, \tag{5}$$

where $D = -\frac{\sqrt{3}d}{at}$ and $A = \frac{\sqrt{3}J}{2t}$ represent the strength constants of the DMI and Heisenberg exchange interaction, respectively, in the continuum magnetic model, effectively derived from the atomic model [42]. It is worth noting that the estimation of the effective thickness $t = 0.2$nm has no impact on λ, and we will demonstrate this later in this paper. After energy minimization, as expected, $\mathbf{M}(\mathbf{r})$ rotates linearly with x, with M_z reaching -1 and 1 on the right side for the states ↑ and ↓, respectively [see Fig. 3(a)].

To explore the dynamic response of the DMI transistor, we then perform magnetization dynamics, which is described by the Landau-Lifshitz-Gilbert equation [44]:

$$\dot{\mathbf{M}} = -\frac{\gamma}{1+\alpha^2}[\mathbf{M} \times \mathbf{H}_{\text{eff}} + \alpha \mathbf{M} \times (\mathbf{M} \times \mathbf{H}_{\text{eff}})], \tag{6}$$

where γ represents the gyromagnetic ratio, α denotes the Gilbert damping constant, and $\mathbf{H}_{\text{eff}} = -\frac{\delta E}{\delta \mathbf{M}}$ denotes the effective magnetic field contributed by the DMI and Heisenberg exchange interaction, which are both counted to the total energy. We begin with $D = 0\text{J/m}^2$ and alternate between setting $D = D_\downarrow$, $D = D_\uparrow$, and $D = D_\downarrow$ sequentially. As illustrated in Fig. 3(b), reproducible magnetization reversal can be achieved in 0.5 ns with $\alpha = 0.1$. Additionally, we perform magnetization dynamics with a series of α (see the Supplemental Material [28]), and the switching time T_S is found to vary inversely with α, i.e., $T_S = C_1/\alpha$, as shown in Fig. 3(c).

Additionally, since the magnetization switching is driven by the DMI torque $\tau_{\text{DMI}} = \mathbf{M} \times \mathbf{H}_{\text{DMI}}$, with $\mathbf{H}_{\text{DMI}}$ denoting the DMI term of $\mathbf{H}_{\text{eff}}$, T_S should be inversely proportional to the strength of the DMI. In addition, though all the magnetic vectors evolve in the mean time (coherently), the spin wave travels throughout the spin spiral and influences the magnetization evolution. In other words, each spin evolves due to the torque from local interactions (since the long-range dipole-dipole interaction is ignored) and then influences the nonneighbored spins step by step. Consequently, T_S should also be directly proportional to the length of the nanoline $|\lambda|/4$ as well as proportional to A/D for $D \ll A$. Thereupon, we perform the magnetization dynamics with a series of D and A (see Fig. S2 in the Supplemental Material [28]) and find out the relationship $T_S = C_2A/D^2$ just as we expected [see Fig. 3(d)]. To sum up, we obtain the relationship:

$$T_S = CA/\alpha D^2. \tag{7}$$

Namely, to fabricate ultrafast DMI transistors, we demand materials with small A, large α, and large D. Another crucial determinant of the switching time is the speed at which polarization switches between the states ↑ and ↓, which is not considered in our simulation. It is worth noting that the effect of thermal fluctuation of the DMI transistor should be considered in a practical device. We have checked that, for a DMI transistor with very small size 24×0.1×0.1 nm, the functionality of the DMI transistor can be easily destroyed by a small thermal fluctuation. By contrast, for the size of 24×10×0.2 nm, which corresponds to a CrN monolayer with a length of 24nm and a width of 10nm, the robustness of the DMI transistor is dramatically enhanced to overcome the thermal fluctuation (see Fig. S3 in the Supplemental Material [28]). Therefore, although we are considering a 1D case, a large enough size of the DMI transistor is vital for the robustness of the DMI transistor against thermal fluctuation.

Furthermore, to extend the universality of our conclusion and take a deep dive into the DMI transistor, we perform analytical calculations to explore the magnetic ground states with a 1D continuum model, in which the uniaxial magnetic anisotropy is also considered. The Hamiltonian of the uniaxial magnetic anisotropy takes the form of $H_{\text{ani}} = -\sum_i k(S_i^z)^2$, where k denotes the strength of uniaxial magnetic anisotropy. Like the Heisenberg exchange interaction, k's for the states ↑ and ↓ are also identical and extracted from our first-principles calculations as $k_\uparrow = k_\downarrow = 0.26$ meV. We assume the propagating direction of magnetization in the 1D continuum model is along the x axis, and the nanoline is with a limited range $[0, L]$. Hence, all nabla operators in Eq. (5) are reduced to a single term representing partial differentiation solely with respect to x. The total-energy functional of the unit local magnetization $\mathbf{m}(x)$ is given by

$$E[\mathbf{m}(x)] = \int_0^L \left[A\left(\frac{\partial \mathbf{m}}{\partial x}\right)^2 + D\left(m_z\frac{\partial m_x}{\partial x} - m_x\frac{\partial m_z}{\partial x}\right) - Km_z^2\right]dx, \tag{8}$$

where the Heisenberg exchange interaction, DMI, and uniaxial magnetic anisotropy are considered and characterized by the strength constants A, D, and $K = \frac{2k}{\sqrt{3}at^2}$, respectively. The magnetic moments lie in the xz plane, so that $\mathbf{m}(x)$ takes the form of $\mathbf{m}(x) = \cos\theta \mathbf{e}_z + \sin\theta \mathbf{e}_x$, where $\theta(x)$ denotes the orientation of the magnetic moment with respect to the z axis.

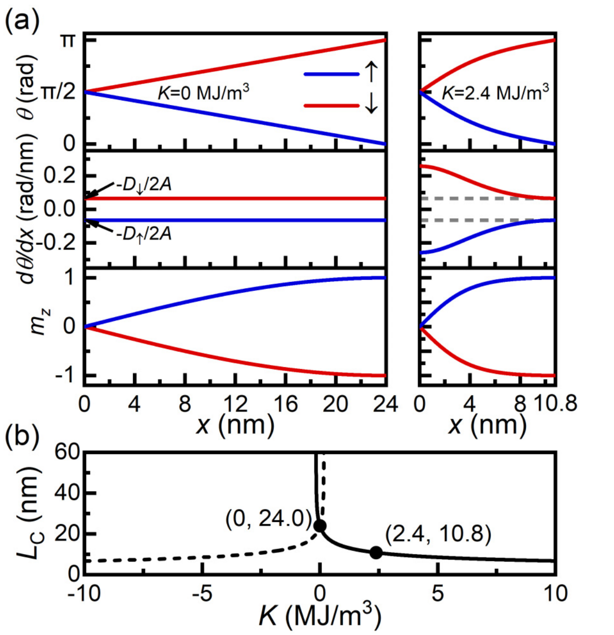

FIG. 4. Solutions of the boundary value problem (BVP) for the magnetic ground state. (a) θ, $d\theta/dx$, and m_z as a function of x, for $K = 0\,\mathrm{MJ/m^3}$ (left panel) and $K = 2.4\,\mathrm{MJ/m^3}$ (right panel). (b) L_C as a function of K (the solid and dashed lines correspond to the results in the configurations of different initial and final phases).

Consequently, Eq. (8) becomes

$$E[\theta(x)] = \int_0^L \left[A\left(\frac{d\theta}{dx}\right)^2 + D\frac{d\theta}{dx} - K\cos^2\theta \right] dx. \tag{9}$$

Through the calculus of variation, the function $\theta(x)$, which minimizes the energy, is given by the following equation:

$$\frac{d^2\theta}{dx^2} = \frac{\cos\theta\sin\theta}{A/K}, \quad x \in (0, L). \tag{10}$$

Consequently, the problem of extremizing the functional transforms into a boundary value problem (BVP) involving a second-order differential equation. Naturally, the boundary conditions read as [43]

$$\theta_x(0) = \theta_x(L) = -\frac{D}{2A}. \tag{11}$$

Here, in our case, the magnetic moment on the left side is fixed toward the x axis, giving rise to the following boundary conditions:

$$\theta(0) = \frac{\pi}{2}, \tag{12a}$$

$$\theta_x(L) = -\frac{D}{2A}. \tag{12b}$$

Substituting the values of D, A, and K, we can numerically solve this BVP and extract the critical length L_C that satisfies $\theta_\uparrow(L_C) = 0$ and $\theta_\downarrow(L_C) = \pi$. As shown in Fig. 4(a), the left panel is the solution with $K = 0\mathrm{J/m^3}$, which is identical to that of the micromagnetic simulation in Fig. 3(a). As expected, θ_{xx} is identical to $0\mathrm{rad/m^2}$ for $K = 0\mathrm{J/m^3}$, resulting in $\theta_x \equiv -\frac{D}{2A}$ and the homogeneous spin-spiral magnetic ground states with $\lambda = \frac{2\pi}{\theta_x} = \frac{2\pi aJ}{d}$. These results are consistent with those obtained from the atomic model above for $d \ll J$. It also explains why the estimation of the effective thickness t keeps λ unchanging. The right panel of Fig. 4(a) is the solution with $K = 2.4\,\mathrm{MJ/m^3}$, which is the value for the CrN monolayer. The critical length L_C of 10.8nm is effectively reduced compared with that with $K = 0\,\mathrm{J/m^3}$. Additionally, $\theta_x(x)$ varies with x and reaches $-\frac{D}{2A}$ on the right side, which is featured by Eq. (10), the boundary condition in Eq. (12b), and $\theta(x)$. We also performed micromagnetic simulation results with uniaxial magnetic anisotropy considered, as shown in Fig. S4 in the Supplemental Material [28], which agrees with our analytical calculation results. Furthermore, we preformed calculations with $-0.1\mathrm{MJ/m^3} < K < 10\,\mathrm{MJ/m^3}$ [35,40,45], where $K > 0$ denotes the out-of-plane magnetic easy axis and vice versa. As shown in Fig. 4(b) (solid curve), L_C increases with K from 10 to $-0.1\,\mathrm{MJ/m^3}$, and the speed also increases. This conclusion suggests that a small and positive K could effectively reduce L_C, resulting in the reducing of the size of the DMI transistor. To be noted, when $K < 0$, L_C increases extremely fast so that we only preform the calculation within a rather limited range for negative K. Nevertheless, when $K < 0$, if we set the initial phase with $\theta(0) = 0$, require the final phase with $\theta_\uparrow(L_C) = -\pi/2$ and $\theta_\downarrow(L_C) = \pi/2$, L_C is actually equivalent with the situation with $K > 0$ in the configuration of $\theta(0) = \pi/2$, $\theta_\uparrow(L_C) = 0$, and $\theta_\downarrow(L_C) = \pi$ [see the dashed curve in Fig. 4(b)]. In other words, by selectively setting the initial and final phases, L_C as well as the length of the DMI transistor can be effectively tuned by the magnetic anisotropy.

It is also worth noting that, in a real device, the fixed layer would not perfectly pin the initial phase when the magnitude of K is sufficiently large. For instance, the ground state of the spin spiral varies with different $\theta(0)$ as well as the corresponding energy $E_0[\theta(x)]$. Therefore, a torque $\tau = \frac{\partial E_0[\theta(x)]}{\partial\theta(0)}$ arises and forces the magnetization of the fixed layer to deviate from the expected orientation and results in an unexpected $\theta(0)$. Contrarily, $E_0[\theta(x)]$ is identical for $\theta(0)$ when K is neglectable; hence, $\theta(0)$ can be well pinned by the fixed layer in this case.

In addition to our previous analysis, we would like to briefly discuss the potential materials and heterostructures, whose DMI vectors can be controlled by external electric fields. Considering the ongoing challenge of finding intrinsic materials that exhibit both FE and FM at room temperature, we propose alternative approaches. For instance, in a FE/FM/FE heterostructure, the FM layer can be polarized by the FE layers through the FE proximity effect [34], and the sandwich structure ensures the degeneracy between the up and down polarization states. Additionally, a dielectric FM material might be temporarily polarized by applying an electric field, giving rise to the volatile DMI transistor with the potential for building ultrafast dynamic logic networks.

III. CONCLUSION

In conclusion, we propose the architecture of a DMI transistor which enables the reproducible magnetization flipping with the electric field by utilizing gate-controlled DMI torque to reverse the chirality of the spin spiral and the magnetization. Through the combination of first-principles calculations, micromagnetic simulations, and analytical calculations, we find that the switching time of the DMI transistor (in subnanoseconds) increases linearly with the magnitude of exchange interaction and decreases linearly with that of the Gilbert damping constant and quadratically with that of DMI. We also find that the size of the DMI transistor (in nanometers) increases linearly with the strength of the exchange interaction, decreases linearly with that of DMI, and can be further tuned by the magnetic anisotropy. The DMI transistor harbors the potential to serve as a fundamental building block of the next-generation logic-in-memory spintronic systems and break the von Neumann bottleneck, with lower energy dissipation, higher speed, and higher integration density. In this paper, we pave the way toward highly desired electric-field control and current-free ultrafast spintronic devices.

ACKNOWLEDGMENTS

This paper is supported by the National Key Basic Research Program of China (Grants No. 2019YFA0308500, No. 2020YFA0309100, and No. 2021YFA1400701), the National Natural Science Foundation of China (Grants No. 12174437, No. 12222414, and No. 12074416), the Strategic Priority Research Program (B) of the Chinese Academy of Sciences (Grant No. XDB33030200), and the Youth Innovation Promotion Association of the Chinese Academy of Sciences (Grant No. Y2022003).

[1] R. Ramesh and L. W. Martin, Electric field control of magnetism: Multiferroics and magnetoelectrics, Riv. Nuovo Cimento **44**, 251 (2021).
[2] S. Manipatruni, D. E. Nikonov, and I. A. Young, Beyond CMOS computing with spin and polarization, Nat. Phys. **14**, 338 (2018).
[3] A. Hirohata, K. Yamada, Y. Nakatani, I.-L. Prejbeanu, B. Diény, P. Pirro, and B. Hillebrands, Review on spintronics: Principles and device applications, J. Magn. Magn. Mater. **509**, 166711 (2020).
[4] P. Dey and J. N. Roy, *Spintronics* (Springer, Singapore, 2021).
[5] M. N. Baibich, J. M. Broto, A. Fert, F. N. Van Dau, F. Petroff, P. Etienne, G. Creuzet, A. Friederich, and J. Chazelas, Giant magnetoresistance of (001)Fe/(001)Cr magnetic superlattices, Phys. Rev. Lett. **61**, 2472 (1988).
[6] M. Julliere, Tunneling between ferromagnetic films, Phys. Lett. A **54**, 225 (1975).
[7] B. Dieny, I. L. Prejbeanu, K. Garello, P. Gambardella, P. Freitas, R. Lehndorff, W. Raberg, U. Ebels, S. O. Demokritov, J. Akerman *et al.*, Opportunities and challenges for spintronics in the microelectronics industry, Nat. Electron. **3**, 446 (2020).
[8] T. Taniyama, Electric-field control of magnetism via strain transfer across ferromagnetic/ferroelectric interfaces, J. Phys.: Condens. Matter **27**, 504001 (2015).
[9] J. J. Wang, J. M. Hu, J. Ma, J. X. Zhang, L. Q. Chen, and C. W. Nan, Full 180° magnetization reversal with electric fields, Sci. Rep. **4**, 7507 (2014).
[10] A. Chen, Y. Zhao, P. Li, X. Zhang, R. Peng, H. Huang, L. Zou, X. Zheng, S. Zhang, P. Miao *et al.*, Angular dependence of exchange bias and magnetization reversal controlled by electric-field-induced competing anisotropies, Adv. Mater. **28**, 363 (2015).
[11] A. K. Biswas, H. Ahmad, J. Atulasimha, and S. Bandyopadhyay, Experimental demonstration of complete 180° reversal of magnetization in isolated Co nanomagnets on a PMN-PT substrate with voltage generated strain, Nano. Lett. **17**, 3478 (2017).
[12] Y. H. Chu, L. W. Martin, M. B. Holcomb, M. Gajek, S. J. Han, Q. He, N. Balke, C. H. Yang, D. Lee, W. Hu *et al.*, Electric-field control of local ferromagnetism using a magnetoelectric multiferroic, Nat. Mater. **7**, 478 (2008).
[13] X. He, Y. Wang, N. Wu, A. N. Caruso, E. Vescovo, K. D. Belashchenko, P. A. Dowben, and C. Binek, Robust isothermal electric control of exchange bias at room temperature, Nat. Mater. **9**, 579 (2010).
[14] S. M. Wu, S. A. Cybart, P. Yu, M. D. Rossell, J. X. Zhang, R. Ramesh, and R. C. Dynes, Reversible electric control of exchange bias in a multiferroic field-effect device, Nat. Mater. **9**, 756 (2010).
[15] S. M. Wu, S. A. Cybart, D. Yi, J. M. Parker, R. Ramesh, and R. C. Dynes, Full electric control of exchange bias, Phys. Rev. Lett. **110**, 067202 (2013).
[16] J. T. Heron, J. L. Bosse, Q. He, Y. Gao, M. Trassin, L. Ye, J. D. Clarkson, C. Wang, J. Liu, S. Salahuddin *et al.*, Deterministic switching of ferromagnetism at room temperature using an electric field, Nature (London) **516**, 370 (2014).
[17] M. Zhu, Y. Li, H. Hu, S. Cui, Y. Qiu, G. Yu, and H.-M. Zhou, Theoretical routes for current-free magnetization switching induced by joint effects of strain and Dzyaloshinskii-Moriya interaction, Appl. Phys. Lett. **121**, 032402 (2022).
[18] Q. Liu, L. Liu, G. Xing, and L. Zhu, Asymmetric magnetization switching and programmable complete Boolean logic enabled by long-range intralayer Dzyaloshinskii-Moriya interaction, Nat. Commun. **15**, 2978 (2024).
[19] D. Yu, Y. Ga, J. Liang, C. Jia, and H. Yang, Voltage-controlled Dzyaloshinskii-Moriya interaction torque switching of perpendicular magnetization, Phys. Rev. Lett. **130**, 056701 (2023).
[20] W. Koshibae and N. Nagaosa, Creation of skyrmions and antiskyrmions by local heating, Nat. Commun. **5**, 5148 (2014).
[21] J. Sampaio, V. Cros, S. Rohart, A. Thiaville, and A. Fert, Nucleation, stability and current-induced motion of isolated magnetic skyrmions in nanostructures, Nat. Nanotechnol. **8**, 839 (2013).
[22] P. Borisov, A. Hochstrat, X. Chen, W. Kleemann, and C. Binek, Magnetoelectric switching of exchange bias, Phys. Rev. Lett. **94**, 117203 (2005).
[23] H. Béa, M. Bibes, F. Ott, B. Dupé, X. H. Zhu, S. Petit, S. Fusil, C. Deranlot, K. Bouzehouane, and A. Barthélémy, Mechanisms of exchange bias with multiferroic $BiFeO_3$ epitaxial thin films, Phys. Rev. Lett. **100**, 017204 (2008).

[24] C. J. Fennie, Ferroelectrically induced weak ferromagnetism by design, Phys. Rev. Lett. **100**, 167203 (2008).
[25] V. Skumryev, V. Laukhin, I. Fina, X. Martí, F. Sánchez, M. Gospodinov, and J. Fontcuberta, Magnetization reversal by electric-field decoupling of magnetic and ferroelectric domain walls in multiferroic-based heterostructures, Phys. Rev. Lett. **106**, 057206 (2011).
[26] Y. Tokunaga, Y. Taguchi, T.-H. Arima, and Y. Tokura, Electric-field-induced generation and reversal of ferromagnetic moment in ferrites, Nat. Phys. **8**, 838 (2012).
[27] J. M. Hu, L. Q. Chen, and C. W. Nan, Multiferroic heterostructures integrating ferroelectric and magnetic materials, Adv. Mater. **28**, 15 (2015).
[28] See Supplemental Material at http://link.aps.org/supplemental/10.1103/PhysRevB.110.094418 for theoretical analyses, micromagnetic simulation results, and methods.
[29] G. Kresse and J. Hafner, *Ab initio* molecular-dynamics simulation of the liquid-metal-amorphous-semiconductor transition in germanium, Phys. Rev. B **49**, 14251 (1994).
[30] G. Kresse and J. Furthmüller, Efficient iterative schemes for *ab initio* total-energy calculations using a plane-wave basis set, Phys. Rev. B **54**, 11169 (1996).
[31] P. E. Blochl, Projector augmented-wave method, Phys. Rev. B **50**, 17953 (1994).
[32] J. P. Perdew, K. Burke, and M. Ernzerhof, Generalized gradient approximation made simple, Phys. Rev. Lett. **77**, 3865 (1996).
[33] A. Vansteenkiste, J. Leliaert, M. Dvornik, M. Helsen, F. Garcia-Sanchez, and B. Van Waeyenberge, The design and verification of MuMax3, AIP Adv. **4**, 107133 (2014).
[34] L. Wang, Q. Feng, Y. Kim, R. Kim, K. H. Lee, S. D. Pollard, Y. J. Shin, H. Zhou, W. Peng, D. Lee *et al.*, Ferroelectrically tunable magnetic skyrmions in ultrathin oxide heterostructures, Nat. Mater. **17**, 1087 (2018).
[35] J. Liang, Q. Cui, and H. Yang, Electrically switchable Rashba-type Dzyaloshinskii-Moriya interaction and skyrmion in two-dimensional magnetoelectric multiferroics, Phys. Rev. B **102**, 220409(R) (2020).
[36] C. Xu, P. Chen, H. Tan, Y. Yang, H. Xiang, and L. Bellaiche, Electric-field switching of magnetic topological charge in type-I multiferroics, Phys. Rev. Lett. **125**, 037203 (2020).
[37] J. Zhang, X. Shen, Y. Wang, C. Ji, Y. Zhou, J. Wang, F. Huang, and X. Lu, Design of two-dimensional multiferroics with direct polarization-magnetization coupling, Phys. Rev. Lett. **125**, 017601 (2020).
[38] G. Chen, M. Robertson, M. Hoffmann, C. Ophus, A. L. Fernandes Cauduro, R. Lo Conte, H. Ding, R. Wiesendanger, S. Blügel, A. K. Schmid *et al.*, Observation of hydrogen-induced Dzyaloshinskii-Moriya interaction and reversible switching of magnetic chirality, Phys. Rev. X **11**, 021015 (2021).
[39] C. E. Fillion, J. Fischer, R. Kumar, A. Fassatoui, S. Pizzini, L. Ranno, D. Ourdani, M. Belmeguenai, Y. Roussigne, S. M. Cherif *et al.*, Gate-controlled skyrmion and domain wall chirality, Nat. Commun. **13**, 5257 (2022).
[40] Z. Shao, J. Liang, Q. Cui, M. Chshiev, A. Fert, T. Zhou, and H. Yang, Multiferroic materials based on transition-metal dichalcogenides: Potential platform for reversible control of Dzyaloshinskii-Moriya interaction and skyrmion via electric field, Phys. Rev. B **105**, 174404 (2022).
[41] T. Moriya, Anisotropic superexchange interaction and weak ferromagnetism, Physi. Rev. **120**, 91 (1960).
[42] C. Ma, K. Jin, C. Ge, E.-J. Guo, C. Wang, and X. Xu, Strong Dzyaloshinskii-Moriya interaction in two-dimensional magnets via lithium absorption, Phys. Rev. B **108**, 134405 (2023).
[43] S. Rohart and A. Thiaville, Skyrmion confinement in ultrathin film nanostructures in the presence of Dzyaloshinskii-Moriya interaction, Phys. Rev. B **88**, 184422 (2013).
[44] T. L. Gilbert, Classics in magnetics a phenomenological theory of damping in ferromagnetic materials, IEEE Trans. Magn. **40**, 3443 (2004).
[45] J. Qi, H. Wang, X. Chen, and X. Qian, Two-dimensional multiferroic semiconductors with coexisting ferroelectricity and ferromagnetism, Appl. Phys. Lett. **113**, 043102 (2018).